Measured limits on amplitude dependence of mechanical loss in substrate-transferred $GaAs/Al_{0.92}Ga_{0.08}As$ coatings

Elizabeth M. Gretarsson*
Wyant College of Optical Sciences, University of Arizona, 1630E. University Blvd., Tucson, Arizona 85721, USA and Embry-Riddle Aeronautical University, 3700 Willow Creek Rd., Prescott, Arizona 86301, USA

Andri M. Gretarsson
Department of Physics and Astronomy, Embry-Riddle Aeronautical University, Prescott, Arizona 86301, USA

Garrett D. Cole
Thorlabs Crystalline Solutions, 114 E Haley St. Suite G, Santa Barbara, California 93101, USA

Gregory M. Harry and Maya M. Kinley-Hanlon
Department of Physics, American University, Washington DC 20016, USA

R. Jason Jones
Wyant College of Optical Sciences, University of Arizona, 1630E. University Blvd., Tucson, Arizona 85721, USA

Steven D. Penn
Hobart and William Smith Colleges, Geneva, New York 14456, USA

(Received 5 January 2022; accepted 17 July 2022; published 2 August 2022)

The standard approach for predicting thermal noise in optical mirrors using the fluctuation-dissipation theorem requires knowledge of the level of all significant sources of mechanical loss occurring at the oscillation amplitudes of thermal noise. Using a gentle nodal suspension system read out by a Michelson interferometer, we tested the amplitude-dependence of loss in $GaAs/Al_{0.92}Ga_{0.08}As$ multilayer optical coatings on silica substrates in the range from just above the rms thermal noise amplitude up to amplitudes typical of ringdown measurements: 10^{-1}–10^{3} picometers. None of the three samples tested showed any significant amplitude dependence over this range.

DOI: 10.1103/PhysRevD.106.042001

I. INTRODUCTION

A. Thermal noise

Brownian noise [1,2] in high-reflectivity optical coatings [3,4] is currently a limiting source of noise in several experiments using ultrastable optical cavities [5–8]. Ringdown measurements [4,9–12] have been used as an effective method for estimating the thermal noise in cavities. A mirror with the substrate and coating of interest is suspended in some way that allows its mechanical modes to be excited. The loss angle, ϕ, for each of the several mechanical modes is measured via a ringdown technique. The loss angle of the mode is the inverse quality factor of the resonance, $\phi = 1/Q$, where $Q = \pi f \tau$, f is the resonant frequency, and τ is the time it takes the amplitude of the oscillation to freely decay to $1/e$ times its initial value [4,13–15]. Typically, the corresponding loss angle of the coating is extracted by applying the ratio of the resonant energy in the coating to the total resonant energy. Finally Levin's approach is then used to estimate the thermal noise in the mirror of interest [4,9–12].

One benefit of ringdown techniques like this is that they interrogate the entire coating. This is important in applications where the beam radius on the mirror is large. Direct measurements of cavity thermal noise typically use small beams and may miss atypical regions of the coating or substrate (damaged, delaminated, etc.) that contribute to the thermal noise at an unusually high level. This is particularly true for gravitational-wave detectors, where coating Brownian noise is expected to be a limiting noise source in the most sensitive detector band between roughly 40 Hz and 100 Hz [7]. Currently, LIGO gravitational wave

*ejesse@email.arizona.edu

detectors use 34 cm diameter mirrors and future detectors will likely require larger mirrors with stricter requirements on coating thermal noise [16–19].

Since most ringdown measurements are made at amplitudes well above the rms thermal motion, application of this method to thermal-noise estimation relies on the assumption that the quality factor is independent of excitation amplitude. Amplitude dependence of the quality factor means that the mode decay is not perfectly exponential. In this paper, we do not extract the loss angle of the coating from the loss angle of the modes. The reason for this is that we are not only looking for material losses within the coating itself. For example, elementary physics shows that rubbing friction (which could occur if the coating has delaminated regions) leads to nonexponential ringdowns. There may also be other intrinsic mechanisms of which we are not yet aware but the measurements presented here would be sensitive to any such mechanism. Here, we present measurements of loss angle ϕ versus excitation amplitude for three samples with *crystalline*, "AlGaAs," coatings. To our knowledge, this represents the first systematic test of amplitude independence of loss associated with any optical coatings.

The goal of ringdown measurements is to estimate the level of all sources of loss relevant to the prediction of thermal noise in optical cavities. For low-loss materials with high thermal conductivity, like the coatings used here, thermoelastic damping is expected to be a major contributor to the overall measured loss [15,20]. The intrinsic material loss of the coating material and thermoelastic loss are both expected to be amplitude independent. Our goal however is to identify or set upper limits on amplitude-dependent sources of loss that may be detectable against such constant-loss backgrounds. The sensitivity of our search for amplitude dependence is therefore set by the systematics of the measurement; in our case, limited by slight nonlinearities in the signal chain.

B. Crystalline coatings

Multilayered gallium arsenide/aluminum gallium arsenide, $GaAs/Al_{0.92}Ga_{0.08}As$ ("AlGaAs") crystalline mirrors are candidates to replace traditional amorphous materials for future LIGO detectors [15,21]. Experiments using crystalline coatings have shown significantly lower loss angles and correspondingly lower thermal noise than traditional dielectric coatings [13,22–26]. These coatings are already used extensively in ultrastable cavities, mostly with mirrors 2.5 cm or smaller in diameter [5]. To be useful in large scale interferometers, coatings must be manufactured on the tens of centimeters diameter scale and maintain the properties achieved on small mirrors.

One concern about the scalability of these coatings is whether the coating can be bonded to the substrate across the entire surface area with the same quality/integrity as smaller coatings. The process of manufacturing crystalline coatings involves growing the coating on a seed crystal, removing it from the seed, and then bonding it to the desired substrate [27]. Defects in that bond, variations in mechanical dissipation across the bond, and other coating defects could increase the elastic loss of the sample and lead to optical scatter. Here we look for losses that vary with the amplitude of vibration as such amplitude dependence has been observed to be associated with rubbing [28]. We are particularly interested in rubbing from possible delaminated regions of the optical coating and purposely employ imperfect coatings for these experiments.

II. MEASUREMENT METHOD

A. The samples

We measured the loss as a function of vibration amplitude in the three multilayer AlGaAs-coated samples shown in Fig. 1. We also measured the loss of an uncoated pure silica sample as a reference for determining the scale of nonlinearity in the signal chain and to set limits on the level of suspension losses and other noncoating related excess losses in the system.

Sample A (76×1 mm), the 'pristine' sample, is an intact coating that was recently received from Thorlabs crystalline solutions. This sample is coated on one side with a thermo-optically optimized design [29], consisting of alternating layers of GaAs and $Al_{0.92}Ga_{0.08}As$. This coating had no visible defects apart from three very small

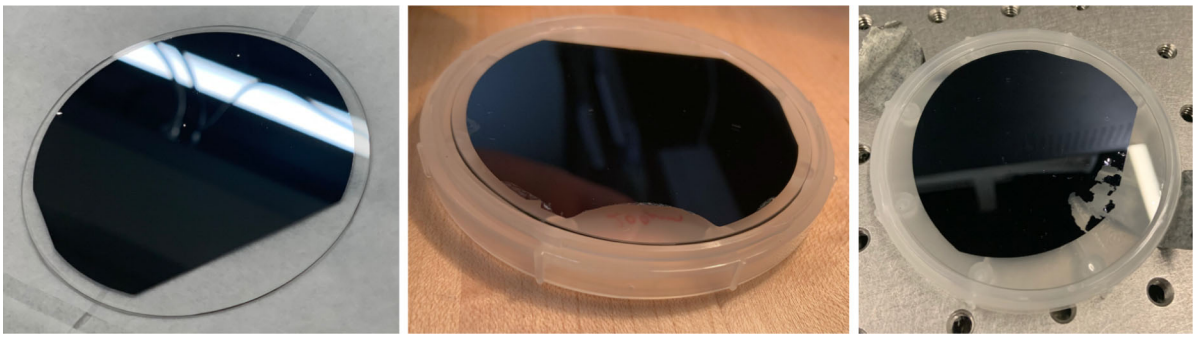

FIG. 1. Images of the three samples. From left to right: Sample A, Sample B, Sample C. The flat sides of the circular coating areas denote the crystal orientation.

crystal defects visible as scattering centers. The coating thickness was 5.9 μm.

Sample B (76 × 1 mm) is coated on one side with with a standard quarter wave (1064/4 nm) stack of alternating layers of GaAs and $Al_{0.92}Ga_{0.08}As$. The coating thickness was 5.9 μm. It was used to test the bond strength between the coating and substrate, which removed sections of coating from the edges. This coating serves as an example of a coating with known edge defects as well as having small surface defects.

Sample C (76 × 1 mm) is coated on one side with a standard quarter wave (1064/4 nm) stack of GaAs and $Al_{0.92}Ga_{0.08}As$. The coating thickness was 5.9 μm. This sample was previously studied as described in [15], where the mechanical loss was measured before and after etching away areas with bond defects. That study found no significant excess loss due to these defects. However, the coating was later badly damaged when compressed air lifted a parts of the coating where etching had previously been performed causing visible delamination and flaking. For this study, it is interesting to compare coatings with varying levels of visible damage since one would expect amplitude dependence from rubbing between the coating and substrate to be most prominent in the most heavily damaged sample.

The uncoated fused silica reference sample was a slightly thicker disk; it had the same 76 mm diameter but was 3 mm thick.

B. A high-sensitivity, Michelson-readout GeNS system

We used a low-noise Michelson interferometric readout to measure the surface movement of the sample during ringdowns. Each sample is balanced on a spherical glass (BK7) lens. This type of configuration is commonly known as a gentle nodal suspension (GeNS) [30,31]. The samples are excited using a comb capacitor placed about 2 mm from the sample surface and driven with an oscillating high voltage at a resonant frequency of the sample. The divergent electric field induces opposite, unequal bound surface charges on the two sides of the disk which induces an oscillating net force. After the mode is excited, the capacitor is turned off and the sample is allowed to ringdown freely. The GeNS suspension only allows excitation of mechanical modes with a node at the location of the support in the center of the sample. All three AlGaAs samples have nominally the same geometry so the resonance frequencies are approximately the same for all the samples. Since the samples are disks, modes with nodal lines along a diameter always have near-degenerate counterparts corresponding to the nodal diameters rotated by half the smallest angle of rotational symmetry. The frequency separation of these degenerate pairs is indicative of a slight geometric asymmetry of the particular sample. For the sake of consistency and to prevent beats, we chose only one of each set of nearly degenerate mode pairs for measurement. Observation with a spectrum analyzer in real time allowed us to ensure that only the chosen mode of a nearly degenerate pair was excited.

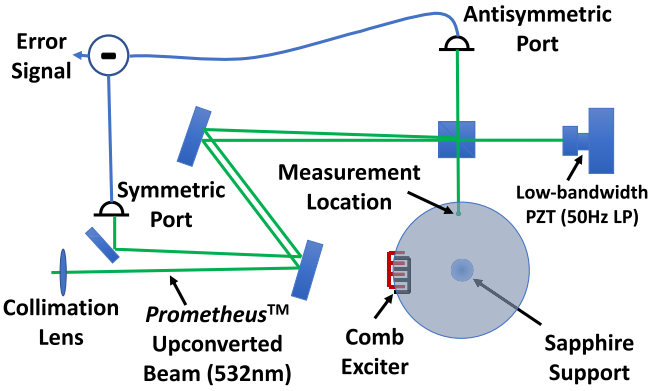

FIG. 2. Top view of the optical layout.

The measurement setup is shown in Fig. 2. The light source was the 532 nm output from a Coherent® Prometheus laser. The beam was collimated, directed into the vacuum chamber through a window, and steered into the Michelson interferometer. The in-vacuum components were mounted on a vibration-isolation platform (model 200 CM-1CV from Minus K Technology). The vacuum was typically pumped to around 5×10^{-7} Torr using a turbo pump backed by a dry scroll pump. The interferometer measured the surface movement at a location approximately 90 degrees around the sample's axis of symmetry from the comb-exciter's location. The end mirror of the other arm of the interferometer was mounted on a piezoelectric transducer (PZT), low-pass filtered at 50 Hz, and used for locking to a fringe center. The symmetric and antisymmetric port beams were directed out of the vacuum chamber to separate photodiodes. The voltages, which were approximately balanced, were subtracted to reduce common-mode noise on the signal which was sent to an SR830 lock-in amplifier for demodulation. The SR830 gain was adjusted so that the ringdown used most of the dynamic range of Data Acquisition Card (DAQ). The error signal was calibrated from the interferometer fringe height by scanning the PZT.

A typical ringdown is shown in Fig. 3. The signal-to-noise ratio was high for most of the ringdowns and the measurements were generally limited in the ringdown tails by digitization noise in the DAQ. To reach lower amplitudes, the sensitivity on the lock in amplifier was increased. The very lowest amplitude measurements were limited by optical noise from the laser.

C. Estimating the sample loss angle, ϕ

For each measurement, the quality factor $Q = \pi f \tau$ was obtained from the ringdown time τ by fitting to a damped sinusoid

$$x(t) = x_0 e^{-t/\tau} \cos(\omega t + \theta), \tag{1}$$

where x_0 is the amplitude, τ is the ringdown time, and θ is an arbitrary phase offset. The sample loss angle is $\phi = 1/Q$. The angular frequency, ω, is the demodulated angular frequency after the lock-in amplifier. It is 2π times the magnitude of the difference between the local oscillator frequency and the excited mode frequency. (The local oscillator frequency was set during measurement so that the ω lay well within the bandwidth set by time constant of the lock-in amplifier. This ensured that possible frequency drift due to temperature changes did not affect the amplitude calibration.)

We acquired each ringdown for a time equal to several ringdown times τ and never less than 2τ. Each data set was cut into approximately 1.5τ lengths for modes below 9 kHz and 2τ lengths for modes above 9 kHz. We found that the standard deviation of measured loss increased rapidly when the cuts were shorter than 1.5τ, so, this was set as the minimum cut length and consequent amplitude resolution. Higher-frequency modes had lower signal-to-noise ratio, so we chose the slightly longer 2τ cut length for those modes.

Any DAQ saturation, which shows up as flat tops on the error signal, was cut from the beginning of the datasets manually, then the datasets were cut into the appropriate lengths and each section was fit to Eq. (1).

D. Eliminating technical sources of amplitude dependence

To improve sensitivity to sources of amplitude dependent loss in the coating, we minimized nonlinearity in the signal chain. We identified two sources of small nonlinearity in the signal chain and modified our analysis to account for them; soft saturation at high amplitudes of surface vibration and digitization at very low error signal voltages.

The soft saturation effect was seen on the error signal as a gentle flattening of the peaks and troughs of the classic Michelson error signal. This was seen only when the amplitude was greater than 1000 pm. It was present with all samples, including the fused silica reference sample. It appears to be a reduction of average fringe contrast due to the angular motion of the beam reflected from the sample. We limited our analysis to amplitudes below 1000 pm to avoid this technical source of amplitude dependence.

The discreteness of digitization affects the lowest voltage portions of ringdowns as shown in the inset of Fig. 3. A graph of the fitted Q versus the starting voltage of the ringdown data shows a strong downward trend at low voltages. This is a pure digitization effect and is independent of the physical vibration amplitude. To quantify the effect, we performed a Monte Carlo simulation which generated noise-free ringdowns of random amplitude and phase but known time constant and demodulation frequency. The simulation digitized the ringdowns at the same levels as our actual DAQ and then ran them through the same fitting algorithm used to analyze measured data. As an example, Fig. 4 shows the measured Qs for the 4308 Hz mode of

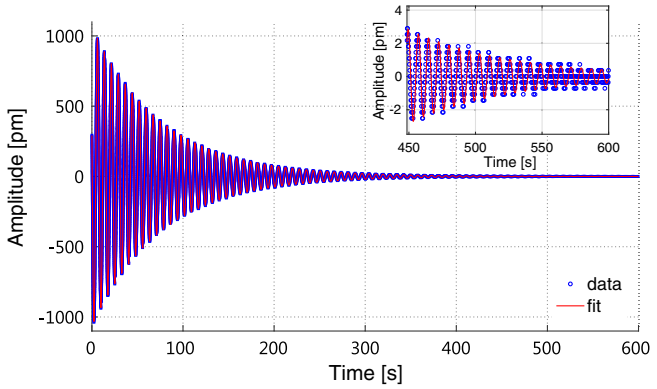

FIG. 3. Typical full ringdown with fit of Sample A. The call out shows a portion of a ringdown and fit where the digitization is a significant fraction of the envelope height.

Sample C and the corresponding Monte Carlo model of fits to model data. The model shows a clear effect from the 12-bit digitization while the data shows a similar reduction but somewhat slower onset. To avoid significant amplitude dependence from this effect, any data set with a maximum voltage below 0.03 V was discarded. The contribution to amplitude dependence from this mechanism is thereby reduced to at most 3% of the measured loss.

III. RESULTS

Since energy lost from different sources is cumulative, loss angles for different loss mechanisms add to produce the total loss. Therefore, we can write the loss in terms of excitation amplitude x to first order as

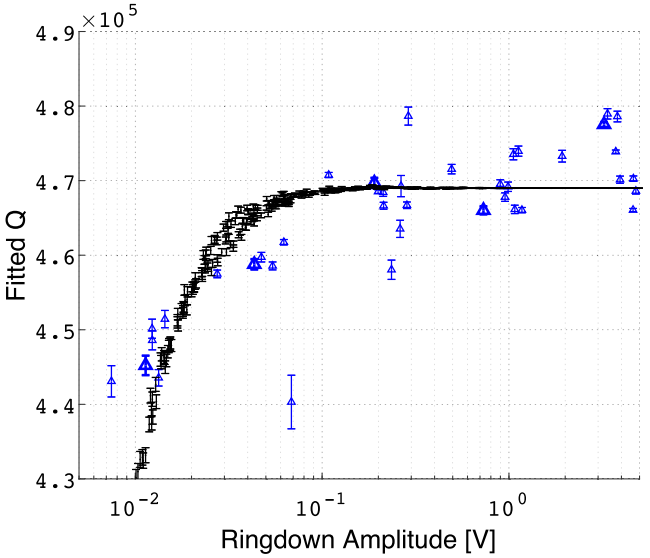

FIG. 4. Fitted Q as a function of maximum voltage of the ringdown. The blue triangles are the fitted Qs, the black dots show the results of the Monte Carlo model of the effect of digitization. The error bars indicate the fitting uncertainties for both the measurements and the model.

$$\phi = \phi_0 + ax, \tag{2}$$

where a is a constant. The amplitude-independent part, ϕ_0, is a combination of several known amplitude-independent losses; coating thermoelastic loss, structural loss, surface loss, etc.

A primary goal of this work was to look for amplitude-dependent sources of loss. The measured loss angles as a function of mean ringdown amplitude are shown in Figs. 5–8. All of these figures indicate that amplitude dependence is small. For reference, the mean thermal excitation amplitude can be estimated from the equipartition theorem $\frac{1}{2}\omega^2\mu x_{\mathrm{max}}^2 = \frac{1}{2}k_B T$, where ω is the angular frequency of the resonance, μ is the modal mass, x_{max} is the excitation amplitude, k_B is Boltzmann's constant, and T is the sample temperature. The modal mass decreases and the resonance frequency increases for higher modes, so the fundamental mode will have the highest average thermal excitation level. For the fundamental mode, μ is on the order of the sample mass, around 10 g, giving $x_{\mathrm{max}} \approx 0.1$ pm. Note that in Figs. 5–8 we are approaching the estimated thermal excitation level. However, it is important to remember that the excitation at the readout point displayed in the figures is expected to be smaller than the mode amplitude due to the fact that the readout point is generally not exactly at an antinode of the resonance.

We searched for any subtle amplitude dependence in two ways. First, we checked whether the measured ϕ had a nonzero power-law dependence on amplitude: $\phi \propto (x/1\ \mathrm{pm})^n$, with $n > 0$. [Such a power-law dependence would in fact contradict our loss model Eq. (2), which is linear, not proportional.] We fit $\log_{10}(\phi)$ vs $\log_{10}(\frac{x}{1\ \mathrm{pm}})$ to a straight line. Figure 9 shows a histogram of the quantity $10 \times n$, or "dB per decade" of amplitude dependence, for all the modes of all the samples. The median $n \approx 0.003$ would only correspond to a 2% change in the loss over the four decades or so measured. That is within the upper bounds on the systematic nonlinearity of the signal chain.

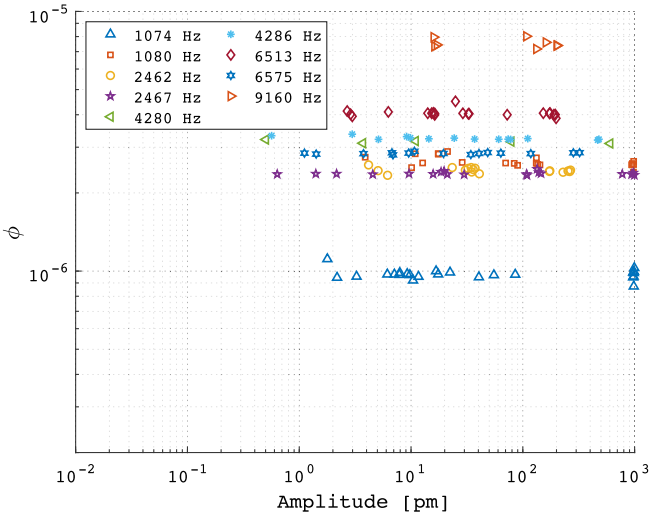

FIG. 6. $\phi = 1/Q$ vs vibration amplitude at readout point for Sample B.

After checking that power-law dependence was insignificant, we fit a straight line to the measured loss as a function of amplitude in order to obtain the slope a in Eq. (2). The distribution of a for all modes of all the samples is shown in Fig. 10. The median amplitude dependence is consistent with zero, $\tilde{a} = (-1.1 \pm 2.2) \times 10^{-10}$. The uncertainty is taken as $\sigma_a/\sqrt{N}$, where $N = 17$ is the total number of modes measured. Therefore, we conclude that evidence for intrinsic amplitude dependence affecting all modes is not present. The nominal median value $\tilde{a}$ is small enough that even at the highest amplitudes measured, around 1 nm,

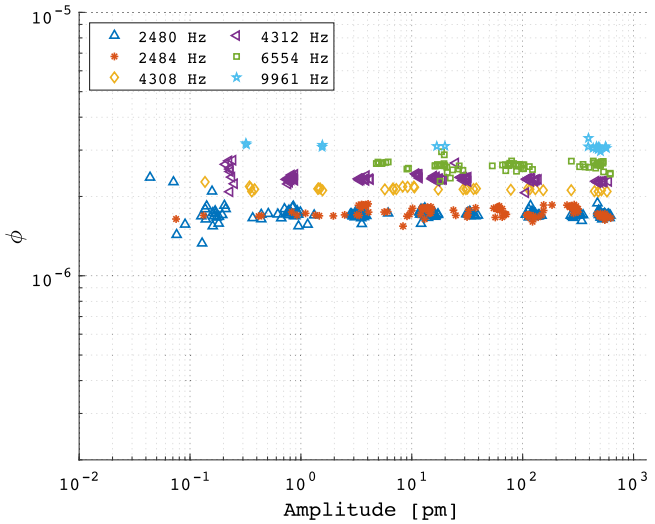

FIG. 5. $\phi = 1/Q$ vs vibration amplitude at readout point for Sample A.

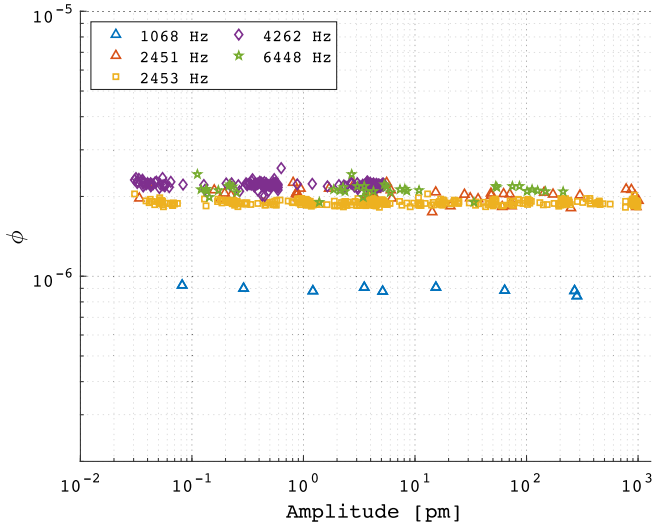

FIG. 7. $\phi = 1/Q$ vs vibration amplitude at readout point for Sample C.

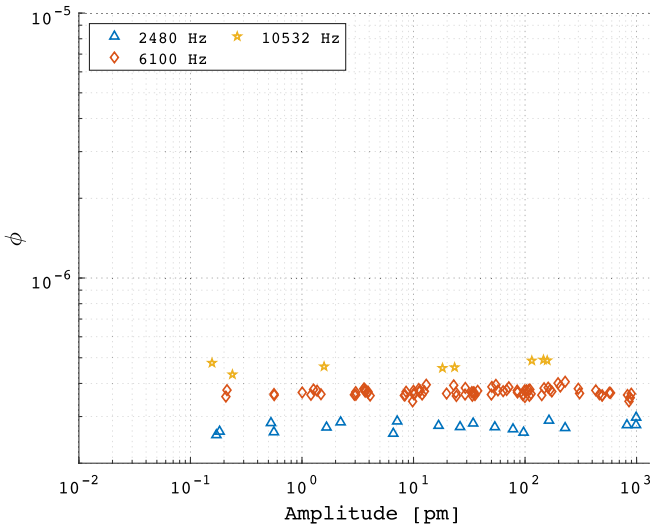

FIG. 8. $\phi = 1/Q$ vs vibration amplitude at readout point for the uncoated, pure silica sample.

it would only imply an 11% change in the loss angles of the lowest-loss modes and considerably less, 3–5%, for other modes. Any amplitude dependence is certainly below the level at which it would impact estimates of coating Brownian noise in optical cavities, including in gravitational-wave interferometers.

A. Loss angle of a thermally excited resonance

Our low-noise Michelson readout system was able to see the fundamental mode of our samples when driven by the

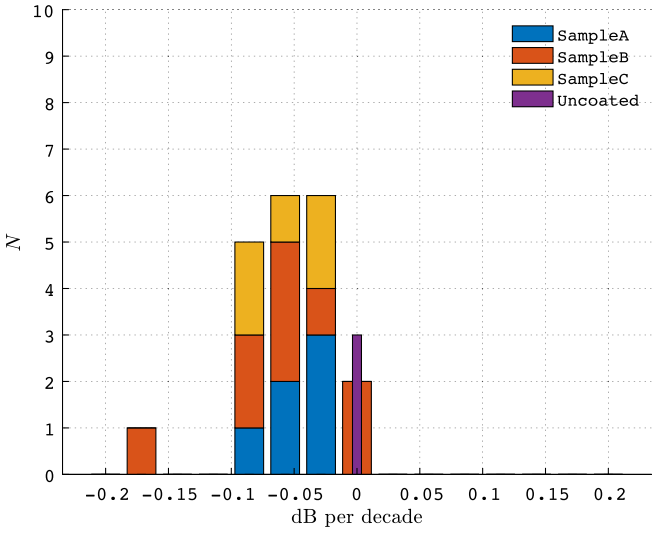

FIG. 9. Histogram of the power-law dependence of all measured modes over all samples. The abscissa is in decibels per decade, or equivalently $10\mathrm{d}\log_{10}(\phi)/\mathrm{d}\log_{10}(\frac{x}{1\ \mathrm{pm}}) = 10 \times n$. The median is -0.031 and the mean is -0.036. The histogram of the coated samples have been combined by stacking. The bars representing the uncoated sample frequencies are not stacked but kept as a separate histogram for comparison.

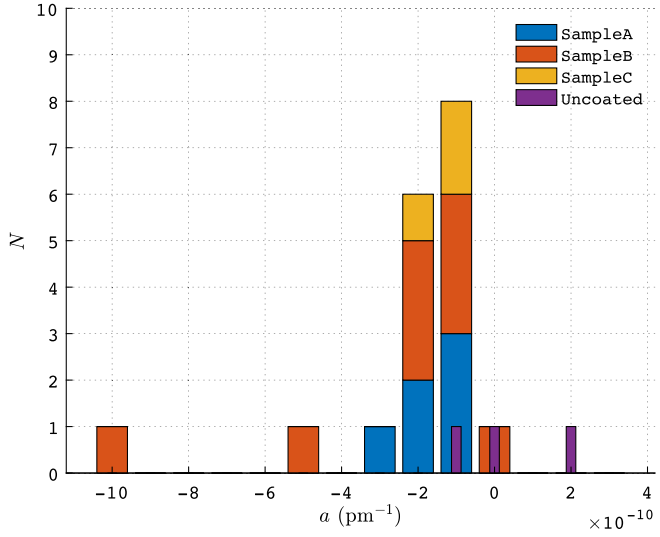

FIG. 10. Histogram of the slopes a of all measured modes over all samples. Median slope is $\tilde{a} = -1.1 \times 10^{-10}$, mean slope is $\bar{a} = -3.5 \times 10^{-10}$. The histogram of the coated samples have been combined by stacking. The bars representing the uncoated sample frequencies are not stacked but kept as a separate histogram for comparison.

intrinsic thermal energy alone. This allowed us to estimate the loss angle at the lowest possible room temperature excitation amplitude of the resonance—the rms thermal excitation amplitude. To make the measurement, we left the sample in a quiet environment for several hours before integrating the signal for 30 minutes with a spectrum analyzer. The amplitude spectral density of the fundamental mode of Sample C is shown in Fig. 11, calibrated in terms of the displacement at the readout point. According to the equipartition theorem, each thermally driven mode contains and average energy of $\frac{1}{2}k_BT$ if no other driving forces are applied. Here, k_B is Boltzmann's constant and T is the temperature in Kelvin. However, if the readout point

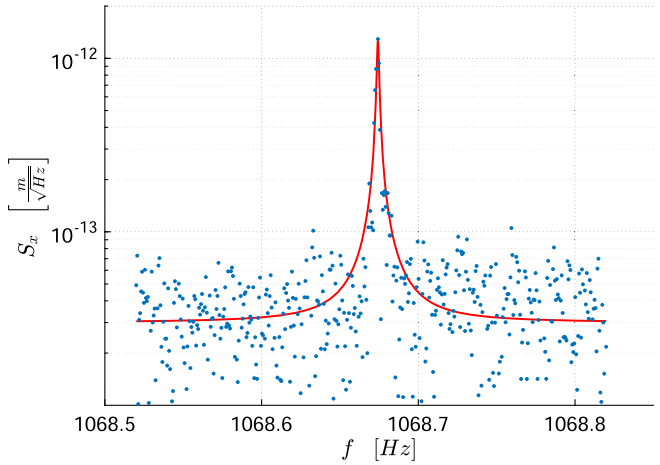

FIG. 11. The thermally-driven 1 kHz mode for Sample C. The red indicates the fitted Lorentzian function.

on the surface is not at an antinode of the mode, the integrated energy in the Lorentzian will appear somewhat less than $\frac{1}{2}k_BT$. We found the energy in this mode as $0.3k_BT$ which is therefore consistent with a thermally driven mode. The full width of the peak at half of the maximum of this mode indicates $\phi_{\text{thermal}} = 1.12 \times 10^{-6}$ which is somewhat greater than the loss estimated from ringdowns. The fitting uncertainties are very small and much lower than the likely inaccuracy due to thermal drift of the resonance peak. The loss angles from ringdowns of this mode covered the amplitudes 0.08 to 283 picometers and had a mean loss angle $\phi_{\text{ringdown}} = 0.89 \pm 0.02 \times 10^{-6}$. The loss angle of the mode showed no significant amplitude dependence over the measured range. As indicated, the ≈20% discrepancy between the loss angles measured from ringdowns and the loss angle measured from the thermal mode is likely due to a slow drift in the resonance frequency over the period of the measurement. Such drifts tend to artificially widen the resonance peak, leading to estimates of the loss that are too high. (It is difficult to estimate how much too high, due to the fact that the temperature change of the sample was not measured. So, the value quoted for ϕ_{thermal} is really an upper limit consistent with ϕ_{thermal}.)

IV. CONCLUSION

The low-noise Michelson readout provides a sufficiently low-noise and high-dynamic range system to measure ringdowns over four orders of magnitude between 0.1 pm and 1000 pm. This covers amplitudes from just above the rms thermal excitation to amplitudes typically associated with ringdown studies. No significant amplitude dependence was found. There was a fair amount of variation between modes but no sample showed significantly more amplitude dependence than another. In particular, neither the average amplitude dependence nor the variation between modes was correlated with the level of visible coating damage.

ACKNOWLEDGMENTS

The authors would like to thank the LIGO optics working group for comments and feedback.

[1] P. R. Saulson, Phys. Rev. D **42**, 2437 (1990).
[2] T. Kessler, T. Legero, and U. Sterr, J. Opt. Soc. Am. B **29**, 178 (2012).
[3] G. Harry, T. P. Bodiya, and R. DeSalvo, *Optical Coatings and Thermal Noise in Precision Measurement* (Cambridge University Press, Cambridge, England, 2012).
[4] S. D. Penn, P. H. Sneddon, H. Armandula, J. C. Betzwieser, G. Cagnoli, J. Camp, D. R. M. Crooks, M. M. Fejer, A. M. Gretarsson, G. M. Harry *et al.*, Classical Quantum Gravity **20**, 2917 (2003).
[5] G. D. Cole, W. Zhang, M. J. Martin, J. Ye, and M. Aspelmeyer, Nat. Photonics **7**, 644 (2013).
[6] A. D. Ludlow, X. Huang, M. Notcutt, T. Zanon-Willette, S. M. Foreman, M. M. Boyd, S. Blatt, and J. Ye, Opt. Lett. **32**, 641 (2007).
[7] A. Buikema, C. Cahillane, G. L. Mansell, C. D. Blair, R. Abbott, C. Adams, R. X. Adhikari, A. Ananyeva, S. Appert, K. Arai *et al.*, Phys. Rev. D **102**, 062003 (2020).
[8] J. M. Robinson, E. Oelker, W. R. Milner, W. Zhang, T. Legero, D. G. Matei, F. Riehle, U. Sterr, and J. Ye, Optica **6**, 240 (2019).
[9] G. M. Harry, A. M. Gretarsson, P. R. Saulson, S. E. Kittelberger, S. D. Penn, W. J. Startin, S. Rowan, M. M. Fejer, D. R. M. Crooks, G. Cagnoli *et al.*, Classical Quantum Gravity **19**, 897 (2002).
[10] Y. Levin, Phys. Rev. D **57**, 659 (1998).
[11] M. Evans, S. Ballmer, M. Fejer, P. Fritschel, G. Harry, and G. Ogin, Phys. Rev. D **78**, 102003 (2008).
[12] Y. Levin, Phys. Lett. A **372**, 1941 (2008).
[13] G. M. Harry, A. M. Gretarsson, P. R. Saulson, S. E. Kittelberger, S. D. Penn, W. J. Startin, S. Rowan, M. M. Fejer, D. R. M. Crooks, G. Cagnoli *et al.*, Classical Quantum Gravity **19**, 897 (2002).
[14] G. M. Harry, M. R. Abernathy, A. E. Becerra-Toledo, H. Armandula, E. Black, K. Dooley, M. Eichenfield, C. Nwabugwu, A. Villar, D. R. M. Crooks *et al.*, Classical Quantum Gravity **24**, 405 (2007).
[15] S. D. Penn, M. M. Kinley-Hanlon, I. A. O. MacMillan, P. Heu, D. Follman, C. Deutsch, G. D. Cole, and G. M. Harry, J. Opt. Soc. Am. B **36**, C15 (2019).
[16] R. Robie, A. Brooks, C. Wipf, K. Arai, and R. Adhikari, Bull. Am. Phys. Soc. (2020), https://meetings.aps.org/Meeting/APR20/Session/D05.5.
[17] D. Reitze *et al.*, Bull. Am. Astron. Soc. **51**, 35 (2019), https://baas.aas.org/pub/2020n7i035.
[18] M. Maggiore, C. Van Den Broeck, N. Bartolo, E. Belgacem, D. Bertacca, M. A. Bizouard, M. Branchesi, S. Clesse, S. Foffa, J. García-Bellido *et al.*, J. Cosmol. Astropart. Phys. 03 (2020) 050.
[19] K. Ackley, V. Adya, P. Agrawal, P. Altin, G. Ashton, M. Bailes, E. Baltinas, A. Barbuio, D. Beniwal, C. Blair *et al.*, Pub. Astron. Soc. Aust. **37**, e047 (2020).
[20] M. M. Fejer, S. Rowan, G. Cagnoli, D. R. M. Crooks, A. Gretarsson, G. M. Harry, J. Hough, S. D. Penn, P. H. Sneddon, and S. P. Vyatchanin, Phys. Rev. D **70**, 082003 (2004).
[21] G. Harry, S. Penn, G. Cole, G. Billingsley, M. Evans, G. Lovelace, and K. Craig, in *Frontiers in Optics/Laser Science* (Optical Society of America, 2018), p. JW4A.77,

http://www.osapublishing.org/abstract.cfm?URI=FiO-2018-JW4A.77.

[22] G. D. Cole, in *Optical Trapping and Optical Micromanipulation IX*, edited by K. Dholakia and G. C. Spalding, International Society for Optics and Photonics (SPIE, 2012), vol. 8458, pp. 28–38, 10.1117/12.931226.

[23] G. D. Cole, S. Gröblacher, K. Gugler, S. Gigan, and M. Aspelmeyer, Appl. Phys. Lett. **92**, 261108 (2008).

[24] G. D. Cole, Y. Bai, M. Aspelmeyer, and E. A. Fitzgerald, Appl. Phys. Lett. **96**, 261102 (2010).

[25] G. D. Cole, I. Wilson-Rae, K. Werbach, M. R. Vanner, and M. Aspelmeyer, Nat. Commun. **2**, 231 (2011).

[26] J. Cripe, N. Aggarwal, R. Lanza, A. Libson, R. Singh, P. Heu, D. Follman, G. D. Cole, N. Mavalvala, and T. Corbitt, Nature (London) **568**, 364 (2019).

[27] G. Cole, LIGO Document G1801024-v2 (2019), https://dcc.ligo.org/LIGO-G1801024.

[28] A. M. Gretarsson, Ph.D. thesis, Syracuse University, 300 North Zeeb Road, Ann Arbor, MI 48106-1346 USA, 2002, https://dcc.ligo.org/LIGO-P1100076.

[29] T. Chalermsongsak, E. D. Hall, G. D. Cole, D. Follman, F. Seifert, K. Arai, E. K. Gustafson, J. R. Smith, M. Aspelmeyer, and R. X. Adhikari, Metrologia **53**, 860 (2016).

[30] E. Cesarini, M. Lorenzini, E. Campagna, F. Martelli, F. Piergiovanni, F. Vetrano, G. Losurdo, and G. Cagnoli, Rev. Sci. Instrum. **80**, 053904 (2009).

[31] A. Roche, A. Markowitz, and R. Adhikari, LIGO Document T1900391-v1, 2019, https://dcc-llo.ligo.org/public/0161/T1900391/001/Anna%20Roche%20LIGO%20project%20proposal.pdf.